ACS Energy LETTERS

http://pubs.acs.org/journal/aelccp

LETTER

Changes from Bulk to Surface Recombination Mechanisms between Pristine and Cycled Perovskite Solar Cells

Juan-Pablo Correa-Baena,[†] Silver-Hamill Turren-Cruz,[†] Wolfgang Tress,[†] Anders Hagfeldt,[*,†] Clara Aranda,[‡] Leyla Shooshtari,[‡,§] Juan Bisquert,[*,‡,∥] and Antonio Guerrero[*,‡]

[†]Laboratory of Photomolecular Science, Institute of Chemical Sciences and Engineering, École Polytechnique Fédérale de Lausanne, CH-1015 Lausanne, Switzerland

[‡]Institute of Advanced Materials (INAM), Universitat Jaume I, 12006 Castelló, Spain

[§]Institute for Nanoscience and Nanotechnology, Sharif University of Technology, Tehran 14588-89694, Iran

[∥]Department of Chemistry, Faculty of Science, King Abdulaziz University, Jeddah, Saudi Arabia

Supporting Information

ABSTRACT: Several aspects on the photophysical characterization of lead halide hybrid organic−inorganic perovskite solar cells remain unsolved. It has been observed that ionic transport and polarization of the interfaces cause very slow changes that interfere with transient measurements with effects that cannot be separated from recombination kinetics. Here we establish a protocol of initial measurement of the solar cell that provides information on recombination characteristics prior to applying any voltage cycling. The photovoltaic device is measured by several methods (photovoltage versus light intensity, open-circuit voltage decay, and impedance spectroscopy) while minimizing the exposure to external voltage stimulus to avoid ionic migration to the contacts. Results are independently confirmed by the analysis of samples with interdigitated electrodes. We show that the high-efficiency perovskite solar cells behave very closely to a bulk recombination ideal photovoltaic model. However, when voltage is scanned to determine current density−voltage curves and impedance spectroscopy at fixed illumination intensity, the cell undergoes significant changes, which we attribute to a dominance of recombination at contacts that have been modified by ionic polarization. Our method provides an effective approach for determining quantitatively the rather significant changes that occur to perovskite solar cells during standard measurements, such as current−voltage curves.

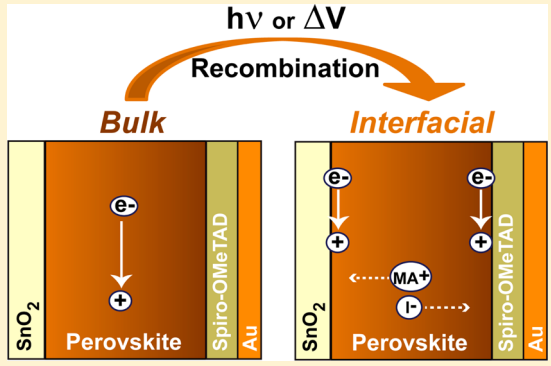

Despite the intensive advance of lead halide hybrid organic−inorganic perovskite solar cells, many important questions about the photophysical characterization still remain unsolved. Of particular importance, transient measurements are often plagued by the interference of ionic transport and polarization that cause very slow changes that cannot be separated from recombination kinetics.[1,2] Certainly, the mere characterization by using different techniques appears to produce structural changes in the perovskite device. For example, it has been reported that external stimulus like light induces structural changes during photoluminescence (PL) and Raman measurements under ambient conditions.[3−6] Similarly, the use of an external electrical field during device characterization promotes ion migration toward the external contact leading to hysteretic behavior observed during cyclic voltammetry (CV) under illumination[7−10] or in dark conditions.[11−13] Figure 1a shows a diagram that represents this ionic migration and ion build up at the external interfaces and how the charge is compensated by the contacts.

The design of measurements that minimize the dose to the external stimuli, which may provide access to the bulk electronic properties of the perovskite layer in a device with contacts, is of utmost importance. One particularly central topic concerning photovoltaic operation of the device is the determination of recombination kinetic constants and their influence on steady-state performance characteristics. In previous related solar technologies, such as dye-sensitized solar cells (DSC) and organic solar cells (OSC),[14,15] it has been

Received: January 19, 2017
Accepted: February 16, 2017
Published: February 16, 2017

DOI: 10.1021/acsenergylett.7b00059
ACS Energy Lett. 2017, 2, 681−688

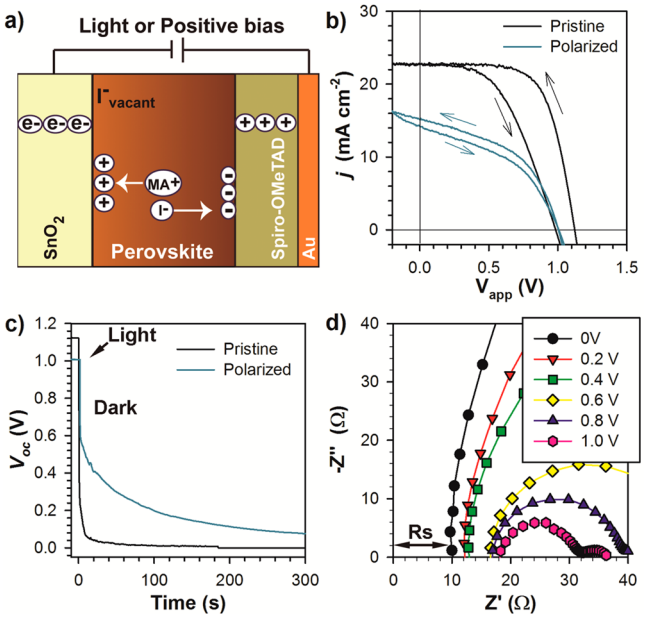

Figure 1. (a) Diagram representing the ion migration under either light conditions or positive bias. (b) $j-V$ curves of a representative pristine device. (c) Open-circuit voltage decay of a pristine and polarized device. (d) Complex impedance plot of a device measured under 1 sun illumination sweeping the voltage from 0 to 1.0 V. It is observed that the series resistance of the devices increases with the applied voltage. The pristine device is polarized by carrying out the IS measurement in panel d; this is 1 sun illumination conditions and different positive bias.

possible to establish unambiguously the recombination resistance. In hybrid perovskite solar cells the carrier lifetime has been described in detail using PL techniques,[16,17] but the electrical measurement method of recombination lifetime in a device with contacts, which is rather common in the other types of solar cells, has not been clearly established.

In this work we present a method to study the bulk properties of the perovskite layer. We will work here with a type of lead halide perovskite solar cells that has been well-described in recent publications and used for detailed impedance spectroscopy (IS) characterization.[18,19] First, devices have been studied by using different standard transient techniques such as cyclic voltammetry, open-circuit voltage decay (OCVD), and impedance spectroscopy. It is shown that all these techniques involve high doses of external stimuli, which induce ion migration toward the contacts. Interestingly, using open-circuit voltages (V_{oc}) under different illumination intensities during IS measurements proves to be much milder and offers information on the intrinsic properties of the perovskite layer.

Analysis by Different Transient Techniques. Devices are prepared in the configuration FTO/SnO_2/perovskite/Spiro-OMeTAD/Au containing a flat conformal layer of SnO_2 by atomic layer deposition (ALD). The perovskite layer presents a mixed formulation to enhance absorption and stability containing Cs/MA/FA/Pb/I/Br (Eg = 1.6 eV), where MA is methylammonium and FA is formamidinium.[20,21] These devices show the following performance parameters measured under reverse sweep direction: power conversion efficiency, η = 18.3%; short-circuit photocurrent density, j_{sc} = 22.6 mA cm^{-2}; open-circuit voltage, V_{oc} = 1.12 V; and fill factor, FF = 74%. The devices incorporate the planar configuration without mesoscopic metal-oxide contact, meaning that we do not have the perovskite infiltrated into a scaffold but a homogeneous thin-film absorber layer.[19] We combine the analysis of the perovskite solar cell with a thin film of the same perovskite on interdigitated electrodes that provides information on the conductivity as a function of light intensity.[22] This second set of devices gives access to the carrier density of perovskite layers from measurements not dependent on photovoltaic devices. To avoid undesirable effects of ambient moisture, the perovskite was protected in the interdigitated configuration with a layer of PMMA. The solar cell devices were stable during storage for weeks in dry atmospheric conditions in the dark.

Transient techniques are initially tested on representative photovoltaic devices that show activated pathways for ions to migrate toward the external interfaces (Figure 1). This type of device represents the worst case scenario where most transient techniques will fail to provide reliable data. The current density−voltage ($j-V$) curves are measured at 1 sun light illumination conditions (AM1.5G) with a step of ΔV = 10 mV and sweep rate of 50 mV/s. Figure 1b shows high hysteresis for a pristine device as the curves in forward and reverse direction are very different. As expected, hysteresis is minimized at still lower scan rates, see the Supporting Information Figure SI1. In addition, other devices with lower hysteresis were produced in the same batch (see Figure SI2), but the following discussion also holds for them. The same pristine sample can be studied by OCVD where the external stimulus is the light (1 sun) over a period of 10 s. After that time, the source of light is switched off and the V_{oc} decay can be monitored as a function of the time. From results of the pristine sample, Figure 1c, it is clear that the V_{oc} of the device decays very fast, and values close to zero are obtained within the first 100 s. It has been reported that longer light-soaking experiments in the range of minutes show significantly different response, indicating that the measurement itself is sufficient to modify the properties of the perovskite layer.[23] Another useful transient technique is impedance spectroscopy, in which a dc voltage is applied to the sample either under light or dark conditions and a small-signal ac voltage perturbation is superimposed over a wide range of frequencies. Therefore, both light and voltage are typically applied to the sample using this technique. Figure 1d shows the complex impedance plot of a device measured at 1 sun light intensity at different dc voltages starting from 0 V up to 1 V. In these plots, the x-axis (Z') is related to resistive elements and the y-axis ($-Z''$) to capacitive elements. The series resistance (R_{series}) of a device, originated by the external contacts, can be monitored using IS as a pure resistance with no capacitive elements. The value can be graphically measured from the intercept with the x-axis of the first capacitive element. The data clearly shows that the R_{series} of the device increases from 10 to 18 Ω during the measurement time as the combined effect of the applied positive dc voltage and the illumination time. The increase in series resistance can be viewed as a further support for ion accumulation at the contacts, as represented in Figure 1a. It is noted that the response of the series resistance with the applied voltage is not linear. We believe that once ions are already present at the extracting interfaces a further increase in the local ion concentration is hindered as there are fewer available sites for ions to move. These ions will increase the recombination kinetics as well, as reported elsewhere.[24] Furthermore, the presence of ions at the external interfaces can lead to chemical reactions at the interfacial level, and this would modify the extraction properties of the selective

DOI: 10.1021/acsenergylett.7b00059
ACS Energy Lett. 2017, 2, 681−688

contacts.[11] It is noted that the actual interfacial chemistry has been rather elusive because of the difficulty and sensitivity requirements for the characterization techniques to offer in situ information. However, some of the previous work suggests that interfacial chemistry may be limiting the device performance. For example, iodide interactions with TiO_2 has been identified to form Ti−I−Pb bond, and this interaction will depend on the local iodide concentration.[25] Alternatively, it has previously been shown that iodide can also react with the oxidized form of Spiro-OMeTAD, leading to the neutral molecule that lacks adequate conductivity, increasing the series resistance.[11] The current results suggest that the chemical reactivity is promoted by light and the required long acquisition times (≈1 h).

Illumination of the device at 1 sun at 1.2 V for 10 min totally modifies the electrical response as discussed for the IS measurements, leading to a very important reduction in performance parameters as shown in the $j-V$ curve (Figure 1b). All performance parameters are severely reduced as well as the hysteresis as most of the mobile ions have been transported toward the contacts by the induced electrical field and therefore became more immobile, possibly because of chemical reactivity at the contact.[11] We note that the power conversion efficiency can be recovered as shown in the Supporting Information and as reported previously.[26] Subsequent OCVD measurement (Figure 1c) clearly indicates that the dynamics of V_{oc} are also modified, and now the decay is much slower, with V_{oc} exceeding 100 mV even after 300 s. It has previously been shown that during OCVD the charging time of the interface can take several minutes, and this requirement is fulfilled in the IS measuring conditions.[23] Indeed, the presence of a very large hole concentration at the interface with the electron extraction layer (i.e., SnO_2) due to accumulation conditions has been reported after using a light bias. The precise nature of ion migration and reactivity at the contacts has been addressed in previous papers, and it is still under debate.[11,27] However, it is clear that the three discussed transient techniques (CV, OCVD, and IS) persistently modify the state of the perovskite solar cell during the measurement itself. Unfortunately, it is not possible to offer a precise time scale for exposure to external stimuli upon which the electrical response is modified. While some devices are very robust and can stand relatively long illumination and polarization voltages, i.e. minutes, other devices seem to be more sensitive and dramatically modify their properties in seconds.

Physical Model. To develop a quantitative methodology that will allow us to assess the performance parameters of the devices, we describe a photovoltaic model for the perovskite solar cell based on standard semiconductor theory.[28,29] We are particularly interested in establishing the deviation from ideality of the solar devices; hence, we introduce in the model a specific nonideal exponent, m_d, and we explore the consequence of this assumption on measurable quantities. We develop the interdependence of different relevant quantities by means of a zero-dimensional model that assumes homogeneous distribution of carriers in the layer thickness d.

The voltage in the solar cell is given by the difference of electrochemical potentials (quasi Fermi levels) of electrons and holes at the respective selective contacts

$$qV = E_{Fn} - E_{Fp} \tag{1}$$

Electron and hole densities obey the following equations in terms of elementary charge q and the thermal energy k_BT

$$n = n_0 \exp[(E_{Fn} - E_{F0})/k_BT] = N_c \exp[-(E_c - E_{Fn})/k_BT] \tag{2}$$

$$p = p_0 \exp[-(E_{Fp} - E_{F0})/k_BT] = N_v \exp[(E_v - E_{Fp})/k_BT] \tag{3}$$

where N_c and N_v are effective densities of states in the conduction and valence band edge, respectively,[29] and we have the product

$$np = n_i^2 \exp(qV/k_BT) \tag{4}$$

$$n_i^2 = N_cN_v \exp(-E_g/k_BT) \tag{5}$$

We describe the bimolecular recombination rate as a function of local carrier densities

$$U_n = B_{rec}[(np)^{1/m_d} - n_i^{2/m_d}] \tag{6}$$

Here, the parameter B_{rec} is a kinetic recombination rate and m_d accounts for the nonideal behavior of recombination that departs from strict molecular law ($m_d = 1$). The recombination current is given by the integral of eq 6 over device thickness

$$j_{rec}(V) = j_0[\exp(qV/m_dk_BT) - 1] \tag{7}$$

The dark diode current is $j_0 = qB_{rec}dn_i^{2/m_d}$. We remark that m_d describes nonideal behavior in the current−voltage curve, which is due to local recombination in the bulk absorber layer, and *not* to effects at the contact interfaces.

The local generation rate by absorbed light flux Φ_{ph} is

$$G = \frac{1}{d}\Phi_{ph} \tag{8}$$

The photocurrent is obtained by integration of the generation rate

$$j_{ph} \approx qGd = q\Phi_{ph} \tag{9}$$

Current−voltage characteristics are described by the equation

$$j(V) = j_{ph} - j_0[\exp(qV/m_dk_BT) - 1] \tag{10}$$

Under intense illumination, the number of photogenerated carriers is greater than native doping density. Electroneutrality implies

$$n = p \tag{11}$$

From eq 4 the electron density depends on voltage as

$$n = n_i \exp(qV/2k_BT) \tag{12}$$

We neglect the constant term in eq 6, and the recombination rate takes the form

$$U_n = B_{rec}n^{2/m_d} \tag{13}$$

The open-circuit condition, $G = U_n$, tells us that

$$n = \left(\frac{1}{dB_{rec}}\Phi_{ph}\right)^{m_d/2} \tag{14}$$

Open-circuit voltage depends on illumination flux as

$$V_{oc} = \frac{m_dk_BT}{q}\ln(\Phi_{ph}) \tag{15}$$

An additive constant has been omitted in eq 15. The conductivity is

DOI: 10.1021/acsenergylett.7b00059
ACS Energy Lett. 2017, 2, 681−688

$$\sigma = q\mu_n n \tag{16}$$

where μ_n is an effective mobility. In the case of an interdigitated electrode illuminated from the top at open-circuit conditions, the conductivity shows the dependence

$$\sigma = q\mu_n \left(\frac{\Phi_{ph}}{dB_{rec}} \right)^{m_d/2} \tag{17}$$

The recombination resistance is defined as

$$R_{rec} = \left(\frac{\partial j}{\partial V} \right)^{-1} \tag{18}$$

Thus

$$R_{rec}(V) = R_{rec0} \exp(-qV/m_d k_B T) \tag{19}$$

So far the voltage has been associated with the splitting of Fermi levels. In the presence of a series resistance it is necessary to apply a correction to the applied voltage at the contacts:

$$V = V_{app} - jR_{series} \tag{20}$$

As mentioned above, the simple model outlined here aims to capture the sources of nonideal behavior in the current−voltage and conductivity measurements, mainly close to open-circuit conditions, associated with a nearly homogeneous distribution of carriers. The model is a simple, useful tool for analyzing if the solar cell characteristics can be well-described just by the photophysics of electron and hole carriers in the bulk, i.e., this model is determined by bulk recombination alone. We do not suggest that this is the general case. Indeed, we remark below that under sustained polarization by applied bias the ionic accumulation causes a large control of recombination at the outer interface, which the above model cannot describe. For example, in the case of strong inhomogeneous distribution of carriers (e.g., for cells with a short diffusion length) a more complex device simulation will also certainly be required.

Analysis of Bulk Properties of the Perovskite Layer. Now that a suitable physical theory has been described, we can proceed to present the measurements and analysis of the two types of devices fabricated in this work. First, in order to study the properties of bulk charge carrier densities, conductivity measurements of the perovskite material were performed on devices with interdigitated electrodes. The device configuration is shown as the inset of Figure 2a where a channel length of 50 μm is observed. The current−voltage characteristics were measured as a function of the light intensity I_0 covering the range from 0.01 to 100 mW/cm^2. The perovskite material clearly shows photoconductivity as previously reported,[22,30,31] and the current of the device increases more than 2 orders of magnitude with the incident light intensity. Conductivity can be calculated by extracting the material resistivity considering the nearly ohmic $j-V$ curves and the geometrical parameters. Figure 2b shows the linear dependence of the conductivity in log scale with the light intensity. A slope of 0.45 can be calculated for data points measured at high illumination conditions, and the ideality factor can be calculated from eq 16 with values close to unity (m_d = 0.9). Very importantly, the slope close to 0.5 from interdigitated electrodes validates the condition $n = p$ assumed in eq 8.

To characterize recombination in the solar cell configuration, we start with the V_{oc} versus light intensity as shown in Figure 3. The curves $V(I_0)$ show different regimes according to the light intensity as reported previously for photovoltaic devices by

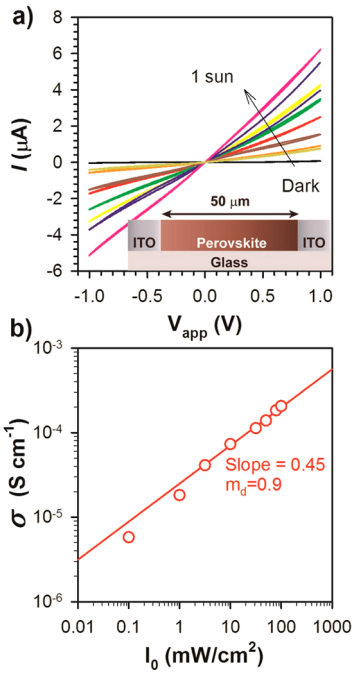

Figure 2. (a) Photocurrent measurements under different illumination conditions for a sample with interdigitated electrode protected with PMMA measured at a scan rate of 50 mV/s. (b) Perovskite conductivity as a function of the light intensity.

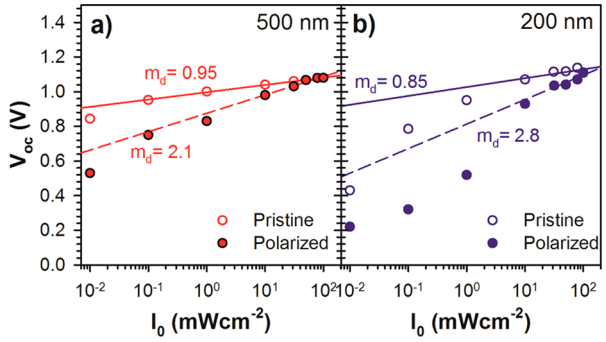

Figure 3. Comparison of V_{oc} dependence with light intensity for photovoltaic devices with different perovskite thickness (200 and 500 nm) measured when pristine and after polarization by applied voltage and light. Data has been fitted to a straight line in the range of 10−100 mW cm^{-2} light intensity.

Zaban and co-workers.[32] The presence of these regimes is better observed in Figure 3b for a thin perovskite layer (200 nm) with a polarized device. At low light intensity the curve is nearly flat, most likely dominated by parasitic shunts. At intermediate light intensity the V_{oc} sharply increases, and at high light intensity the V_{oc} moderately increases, which is typically observed for thin-film solar cells. In perovskite solar cells it is reported that this region becomes independent of the type of contact.[32] We expect that the logarithmic dependence observed at high intensity is primarily due to bulk recombination. Here, the V_{oc} dependence has been analyzed for pristine devices and for devices that have been polarized. The data has been fitted to a straight line in the range of 10−100 mW cm^{-2} light intensity. Some representative data is shown in Figure 3 for two devices prepared with different perovskite thickness. It is observed that the $V(I_0)$ curve depends significantly on whether the device has been polarized

DOI: 10.1021/acsenergylett.7b00059
ACS Energy Lett. 2017, 2, 681−688

by illumination at 1 sun at 1.2 V for 10 min. Pristine devices show V_{oc} reduction of ≈60 mV when the light intensity is decreased 1 order of magnitude, corresponding to nearly ideal behavior of bimolecular recombination. Alternatively, polarized devices show a much more prominent dependence with a reduction of 100−180 mV under the same illumination range. This result is a clear sign that polarized devices suffer from activated recombination pathways. The ideality factor can be calculated from eq 15, and m_d values close to 1 are observed for pristine devices, similar to values observed for interdigitated electrodes. Alternatively, polarized devices show ideality factors exceeding 2.

Additionally, IS measurements have been performed on pristine devices to study the recombination properties. IS measurements were carried out under different light illumination conditions at V_{oc} as described above to avoid the use of external applied voltages, which could modify the external interfaces. For this reason, measurement times were also minimized by restricting the lower-frequency limit to avoid undesirable light-induced chemical reactions with measurements starting in the dark and moving toward high illumination conditions. At the end of the IS measurements, the $j-V$ response is confirmed to be similar to that of a pristine device. By following this methodology, we will show that the high-frequency response is related to the recombination resistance of the bulk of the perovskite layer. Raw data on complex impedance plot and capacitance versus frequency plots are shown in the Supporting Information (Figure SI3), and the R_{series} does not change during the measurement as previously described. IS spectra show two arcs in the complex impedance plot as expected for a device with optimized extraction layers. Data can be fitted to the equivalent circuit previously reported (Figure 4a).[19,33] In this model, both R_1 and C_1 are related to the perovskite/extraction layer interface and arise in the low-frequency region. The capacitance C_{bulk} measured in the high-frequency region is related to the dielectric properties of the perovskite layer.[19] The nature of the associated resistance (R_{rec}) leading to the high-frequency arc in the complex impedance plot is not totally clear. Zarazua et al. have recently shown that for devices with previous electrical and optical history (i.e., previously the $j-V$ curve has been measured) the resistance is related to surface recombination processes at the external interfaces.[33] Alternatively, for pristine devices that have not been previously polarized, the resistance depends exclusively on the bulk properties of the perovskite layer, as will be described below.

In Figure 4b it is observed that R_{rec} decreases exponentially with the light intensity, providing higher V_{oc} at high light intensities. Open symbols indicate that the IS measurements have been carried out under the V_{oc} mild conditions (see Methods). As described in Figure 3, the V_{oc} does not change much over an entire order of magnitude in light intensity. Using eq 19, an ideality factor approaching unity is obtained (m_d = 1.1). Very importantly, this value is very similar to that obtained in interdigitated electrodes, suggesting that the resistance arises from the bulk properties of the perovskite layer. After this IS measurement, the $j-V$ curve of the device is measured, and Figure 4c shows rather marked hysteresis behavior. Subsequently, the IS response of the device is measured at constant illumination (1 sun). It has already been shown that the applied dc bias and constant light illumination used for impedance spectroscopy modifies the concentration of ions accumulated at the interfaces.[34] Indeed, variations in series resistance of devices

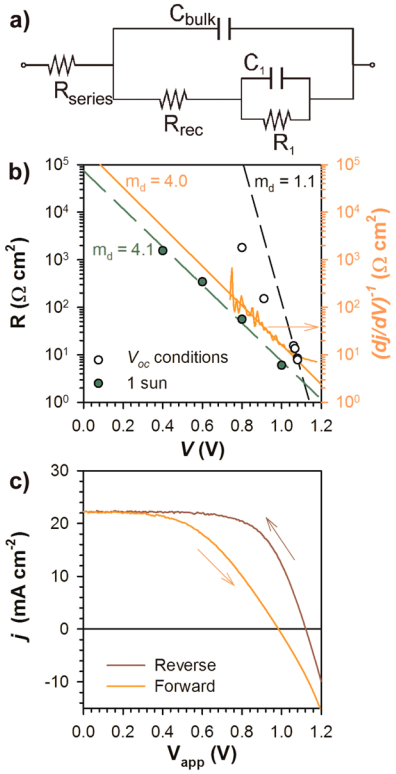

Figure 4. (a) Equivalent circuit used to fit the impedance data. (b) Fitting results for the high-frequency resistive response (R_{rec}) of IS measurements. Open circles correspond to measurements carried out at V_{oc} conditions under different light intensities. Green circles are obtained from measurements at 1 sun light intensity at different applied DC voltage. First derivate of current with the applied voltage is shown for comparison. The applied voltage has been corrected to take into account the voltage drop at the external contacts due to the R_{series}. (c) $j-V$ response measured in the forward and reverse direction of the device analyzed by impedance spectroscopy under constant illumination (1 sun) in panel b.

can be observed, indicating that large modifications have been induced. Interestingly, for measurements carried out at 1 sun light intensity (green circles) with applied voltage, the slope of the straight line defined by the different data points is rather different from measurements performed at V_{oc} conditions and provides an ideality factor of m_d = 4.0. It is important to note that the voltage has been corrected to account for the voltage drop that takes place at the contacts due to the series resistance of the device, eq 20, where the R_{series} has been obtained from fitting of the IS measurements. In any case, this high-frequency resistance does seem to be a real recombination resistance. Equation 18 defines R_{rec} as the first derivative of the current density with the voltage, and this function is plotted for the same device measured under 1 sun light illumination in Figure 4b (orange line). To obtain this curve, we applied direct analysis of the $j-V$ curve in Figure 4c using eq 18 with correction for the series resistance for the measurement under forward conditions (orange trace). As can be observed, the slope of the straight line for data points obtained from the forward scan and close to V_{oc} of the device coincides with that from the R_{rec} measured from the impedance data. Therefore, we can conclude that the resistance associated with the high-frequency arc is a real recombination resistance that can provide kinetic information. The match of values indicates that this exponent directly controls the fill factor and hence the

DOI: 10.1021/acsenergylett.7b00059
ACS Energy Lett. 2017, 2, 681−688

steady-state performance of the perovskite cell. However, the value m_d = 4.0 is very high and indicates that the physical model outlined above in which m_d is explained by nonideal recombination, eq 6, is not valid when the applied voltage is inducing additional causes of nonideal behavior that have been caused by polarization procedures. We suggest that the polarization by a bias voltage is affecting severely the operation of contacts because of ion migration effects that lead to the nonideal exponent m_d = 4.0. In this case, the proposed model based on bulk quantities does not hold because interfacial and possibly defect-mediated recombination becomes dominant, as shown by Zarazua et al.[33]

Finally, we can compare in Figure 5 the impedance response of pristine and polarized devices measured under V_{oc}

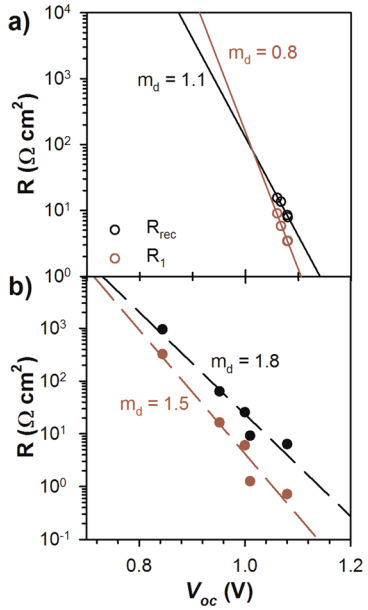

Figure 5. Fitting results for resistances associated with process in high- and low-frequency range for pristine (a) and polarized (b) devices.

conditions, in which the scan of dc bias is avoided, decreasing the ion migration effect. In this analysis, special attention is paid to both resistive processes observed at high and low frequency. Alternatively, the ideality factor m_d can be calculated from the slopes of the straight lines defined by the resistances of the high- and low-frequency regions. Pristine devices show ideality factors close to unity for both high and low resistances, similar to those observed for interdigitated electrodes. On the other hand, polarized devices show ideality factors considerably higher, between 1.5 and 1.8, with values closer to those previously reported for lower-efficiency devices.[33] Therefore, one can conclude that the resistances in pristine devices correspond to the recombination properties in the bulk of the perovskite layer, whereas in prepolarized devices, recombination is taking place close to the external contacts, as reported previously.

In conclusion, we have adopted a series of characterization measurements in which a pristine, previously untreated perovskite solar cell is under a pure bulk recombination regime. A number of different measurements indicate that carrier density and open-circuit voltage are largely controlled by the bulk charge density which is established by equilibrium of generation−recombination, providing a close to ideal exponent of recombination and diode curve. However, when the solar cell is forced to establish charge extraction by applied bias voltage, the contacts become modified and take a leading role in the subsequent operational properties of the solar cell. Overall we show that the electrical properties of the bulk perovskite layer can be probed by reducing the exposure of the photovoltaic device to external stimulus able to induce ion migration toward the external contacts. If the device is exposed to light or electrical field, ions will build up at the contacts and the major electrical response will be dominated by the interfaces of the perovskite with the charge transport layers. Therefore, transient measurements will be influenced by the interference of ionic transport and ionic redistribution that causes very slow changes that cannot be separated from recombination kinetics. Alternatively, if during the measurement electrical fields are minimized, low light intensities are used, and measuring times are reduced, pure electrical response of the perovskite layer appears with no interferences from the external contacts.

METHODS

Electron-Selective Layer Preparation. F:SnO_2 substrates were first wiped with acetone and then cleaned for 10 min in piranha solution (H_2SO_4:H_2O_2 = 3:1) followed by 10 min in a plasma cleaner prior to ALD deposition.

SnO_2 was deposited at 118 °C using tetrakis(dimethylamino)tin(IV) (TDMASn, 99.99%-Sn, Strem Chemicals INC) and ozone at a constant growth rate of 0.065 nm/cycle measured by ellipsometry. TDMASn was held at 65 °C. Ozone was produced by an ozone generator ((AC-2025, IN USA Incorporated) fed with oxygen gas (99.9995% pure, Carbagas) producing a concentration of 13% ozone in O_2. Nitrogen was used as a carrier gas (99.9999% pure, Carbagas) with a flow rate of 10 sccm.

Perovskite Precursor Solution and Film Preparation. Mixed-cation lead mixed-halide perovskite solution was prepared from a precursor solution made of FAI (1 M, Dyesol), PbI_2 (1.1 M, TCl), MABr (0.2 M, Dyesol), and $PbBr_2$ (0.22 M, TCl) in a 4:1 (v:v) mixture of anhydrous DMF:DMSO (Acros). A 1.5 M stock solution of CsI (abcr GmbH) in DMSO was added to the above solution in a 5:95 volume ratio. The triple-cation perovskite solution was deposited through a two-step spin coating program (10 s at 1000 rpm and 20 s at 6000 rpm) with dripping of chlorobenzene as antisolvent[35,36] during the second step, 5 s before the end. All the perovskite layers were annealed at 100 °C for 45 min.

The spiro-OMeTAD (Merck) solution (70 mM in chlorobenzene) was spun at 4000 rpm for 20 s. The spiro-OMeTAD was doped at a molar ratio of 0.5, 0.03, and 3.3 with bis(trifluoromethylsulfonyl)imide lithium salt (Li-TFSI, Sigma-Aldrich), tris(2-(1H-pyrazol-1-yl)-4-*tert*-butylpyridine)-cobalt-(III) tris(bis(trifluoromethylsulfonyl)imide) (FK209, Dyenamo), and 4-*tert*-butylpyridine (TBP, Sigma-Aldrich), respectively.[37−39] For one experiment, the Li concentration was varied from 0 to 1 molar ratio (0 to 100%). As a last step, 70−80 nm of gold top electrode was thermally evaporated under high vacuum.

Interdigitated electrodes were purchased from Ossila (Code: S161). Because of the use of a bottom configuration of the interdigitated electrode, the geometrical area was calculated from the contact area between the ITO and the perovskite layer (1.50×10^{-12} cm^2). According to the supplied ITO thickness (100 nm) and the geometry of the electrode, this involves five fingers each 30 mm in length.

DOI: 10.1021/acsenergylett.7b00059
ACS Energy Lett. 2017, 2, 681−688

Devices were measured under different illumination conditions using a Xe lamp (Oriel) with 1.5 AM filter in ambient at relative humidity of 30%. The light intensity was adjusted to 100 mW cm^{-2} sunlight intensity using a calibrated Si solar cell. Different light conditions were generated using reflective optical filters with a wide range of neutral densities (OD = 0.1−4). Prior to the measurements, devices were not exposed to any light-soaking process, and devices were not preconditioned by using an external bias. This special precaution was taken into consideration to avoid the effect of modification of the external interfaces due to ionic movements. Electrical measurements were carried out using a potentiostat equipped with a frequency analyzer module (Autolab PGSTAT30). Impedance spectroscopy measurements were carried out under two set of conditions: 1) Constant illumination and 2) V_{oc} under variable light intensity. Under constant illumination the device is illuminated at 100 mW cm^{-2} and a DC bias is applied from 0 V to 1.2 V with steps of 0.2 V. Experiments were carried out at a frequency range between 1 MHz and 50 mHz. Using these frequency conditions, each measurement at one voltage or illumination condition takes about 5 min. Impedance spectroscopy data was fitted using the equivalent circuit previously described in our group.[19]

■ ASSOCIATED CONTENT

Supporting Information

The Supporting Information is available free of charge on the ACS Publications website at DOI: 10.1021/acsenergylett.7b00059.

Current−voltage and impedance spectroscopy measurements (PDF)

■ AUTHOR INFORMATION

Corresponding Authors

*E-mail: anders.hagfeldt@epfl.ch.
*E-mail: bisquert@uji.es.
*E-mail: aguerrer@uji.es.

ORCID

Juan-Pablo Correa-Baena: 0000-0002-3860-1149
Juan Bisquert: 0000-0003-4987-4887

Notes

The authors declare no competing financial interest.

■ ACKNOWLEDGMENTS

We acknowledge funding from MINECO of Spain under Project MAT2016-76892-C3-1-R and Generalitat Valenciana Project PROMETEOII/2014/020. A.G. thanks the Spanish Ministerio de Economía y Competitividad for a Ramón y Cajal Fellowship (RYC-2014-16809).

■ REFERENCES

(1) Bertoluzzi, L.; Sanchez, R. S.; Liu, L.; Lee, J.-W.; Mas-Marza, E.; Han, H.; Park, N.-G.; Mora-Sero, I.; Bisquert, J. Cooperative kinetics of depolarization in $CH_3NH_3PbI_3$ perovskite solar cells. *Energy Environ. Sci.* **2015**, *8*, 910−915.

(2) Gottesman, R.; Zaban, A. Perovskites for Photovoltaics in the Spotlight: Photoinduced Physical Changes and Their Implications. *Acc. Chem. Res.* **2016**, *49*, 320−329.

(3) deQuilettes, D. W.; Zhang, W.; Burlakov, V. M.; Graham, D. J.; Leijtens, T.; Osherov, A.; Bulovic, V.; Snaith, H. J.; Ginger, D. S.; Stranks, S. D. Photo-induced halide redistribution in organic-inorganic perovskite films. *Nat. Commun.* **2016**, *7*, 11683.

(4) Galisteo-López, J. F.; Anaya, M.; Calvo, M. E.; Míguez, H. Environmental Effects on the Photophysics of Organic−Inorganic Halide Perovskites. *J. Phys. Chem. Lett.* **2015**, *6*, 2200−2205.

(5) Zhou, Y.; Garces, H. F.; Padture, N. P. Challenges in the ambient Raman spectroscopy characterization of methylammonium lead triiodide perovskite thin films. *Front. Optoelectron.* **2016**, *9*, 81−86.

(6) Ledinský, M.; Löper, P.; Niesen, B.; Holovský, J.; Moon, S.-J.; Yum, J.-H.; De Wolf, S.; Fejfar, A.; Ballif, C. Raman Spectroscopy of Organic−Inorganic Halide Perovskites. *J. Phys. Chem. Lett.* **2015**, *6*, 401−406.

(7) Unger, E. L.; Hoke, E. T.; Bailie, C. D.; Nguyen, W. H.; Bowring, A. R.; Heumuller, T.; Christoforo, M. G.; McGehee, M. D. Hysteresis and transient behavior in current-voltage measurements of hybrid-perovskite absorber solar cells. *Energy Environ. Sci.* **2014**, *7*, 3690−3698.

(8) Li, C.; Tscheuschner, S.; Paulus, F.; Hopkinson, P. E.; Kießling, J.; Köhler, A.; Vaynzof, Y.; Huettner, S. Iodine Migration and its Effect on Hysteresis in Perovskite Solar Cells. *Adv. Mater.* **2016**, *28*, 2446−2454.

(9) Snaith, H. J.; Abate, A.; Ball, J. M.; Eperon, G. E.; Leijtens, T.; Noel, N. K.; Stranks, S. D.; Wang, J. T.-W.; Wojciechowski, K.; Zhang, W.; et al. Anomalous Hysteresis in Perovskite Solar Cells. *J. Phys. Chem. Lett.* **2014**, *5*, 1511−1515.

(10) Tress, W.; Marinova, N.; Moehl, T.; Zakeeruddin, S. M.; Nazeeruddin, M. K.; Gratzel, M. Understanding the rate-dependent J-V hysteresis, slow time component, and aging in $CH_3NH_3PbI_3$ perovskite solar cells: the role of a compensated electric field. *Energy Environ. Sci.* **2015**, *8*, 995−1004.

(11) Carrillo, J.; Guerrero, A.; Rahimnejad, S.; Almora, O.; Zarazua, I.; Mas-Marza, E.; Bisquert, J.; Garcia-Belmonte, G. Ionic reactivity at contacts and aging of methylammonium lead triiodide perovskite solar cell. *Adv. Energy Mater.* **2016**, *6*, 1502246.

(12) Almora, O.; Guerrero, A.; Garcia-Belmonte, G. Ionic charging by local imbalance at interfaces in hybrid lead halide perovskites. *Appl. Phys. Lett.* **2016**, *108*, 043903.

(13) Garcia-Belmonte, G.; Bisquert, J. Distinction between Capacitive and Noncapacitive Hysteretic Currents in Operation and Degradation of Perovskite Solar Cells. *ACS Energy Lett.* **2016**, *1*, 683−688.

(14) Bisquert, J.; Fabregat-Santiago, F.; Mora-Seró, I.; Garcia-Belmonte, G.; Giménez, S. Electron lifetime in dye-sensitized solar cells: theory and interpretation of measurements. *J. Phys. Chem. C* **2009**, *113*, 17278−17290.

(15) Garcia-Belmonte, G.; Boix, P. P.; Bisquert, J.; Sessolo, M.; Bolink, H. J. Simultaneous determination of carrier lifetime and electron density-of-states in P3HT:PCBM organic solar cells under illumination by impedance spectroscopy. *Sol. Energy Mater. Sol. Cells* **2010**, *94*, 366−375.

(16) Yamada, Y.; Nakamura, T.; Endo, M.; Wakamiya, A.; Kanemitsu, Y. Photocarrier Recombination Dynamics in Perovskite $CH_3NH_3PbI_3$ for Solar Cell Applications. *J. Am. Chem. Soc.* **2014**, *136*, 11610−11613.

(17) Johnston, M. B.; Herz, L. M. Hybrid Perovskites for Photovoltaics: Charge-Carrier Recombination, Diffusion, and Radiative Efficiencies. *Acc. Chem. Res.* **2016**, *49*, 146−154.

(18) Correa-Baena, J. P.; Steier, L.; Tress, W.; Saliba, M.; Neutzner, S.; Matsui, T.; Giordano, F.; Jacobsson, T. J.; Srimath Kandada, A. R.; Zakeeruddin, S. M.; Petrozza, A.; Abate, A.; Nazeeruddin, M. K.; Gratzel, M.; Hagfeldt, A. Highly efficient planar perovskite solar cells through band alignment engineering. *Energy Environ. Sci.* **2015**, *8*, 2928−2934.

(19) Guerrero, A.; Garcia-Belmonte, G.; Mora-Sero, I.; Bisquert, J.; Kang, Y. S.; Jacobsson, T. J.; Correa-Baena, J.-P.; Hagfeldt, A. Properties of Contact and Bulk Impedances in Hybrid Lead Halide Perovskite Solar Cells Including Inductive Loop Elements. *J. Phys. Chem. C* **2016**, *120*, 8023−8032.

(20) Saliba, M.; Matsui, T.; Seo, J.-Y.; Domanski, K.; Correa-Baena, J.-P.; Nazeeruddin, M. K.; Zakeeruddin, S. M.; Tress, W.; Abate, A.; Hagfeldt, A.; et al. Cesium-containing triple cation perovskite solar

DOI: 10.1021/acsenergylett.7b00059
ACS Energy Lett. 2017, 2, 681−688

cells: improved stability, reproducibility and high efficiency. *Energy Environ. Sci.* **2016**, *9*, 1989−1997.
(21) Anaraki, E. H.; Kermanpur, A.; Steier, L.; Domanski, K.; Matsui, T.; Tress, W.; Saliba, M.; Abate, A.; Gratzel, M.; Hagfeldt, A.; et al. Highly efficient and stable planar perovskite solar cells by solution-processed tin oxide. *Energy Environ. Sci.* **2016**, *9*, 3128−3134.
(22) Sveinbjörnsson, K.; Aitola, K.; Zhang, X.; Pazoki, M.; Hagfeldt, A.; Boschloo, G.; Johansson, E. M. J. Probing Photocurrent Generation, Charge Transport, and Recombination Mechanisms in Mesostructured Hybrid Perovskite through Photoconductivity Measurements. *J. Phys. Chem. Lett.* **2015**, *6*, 4259−4264.
(23) Gottesman, R.; Lopez-Varo, P.; Gouda, L.; Jimenez-Tejada, J. A.; Hu, J.; Tirosh, S.; Zaban, A.; Bisquert, J. Dynamic Phenomena at Perovskite/Electron-Selective Contact Interface as Interpreted from Photovoltage Decays. *Chem.* **2016**, *1*, 776−789.
(24) Zarazua, I.; Han, G.; Boix, P. P.; Mhaisalkar, S.; Fabregat-Santiago, F.; Mora-Seró, I.; Bisquert, J.; Garcia-Belmonte, G. Surface Recombination and Collection Efficiency in Perovskite Solar Cells from Impedance Analysis. *J. Phys. Chem. Lett.* **2016**, *7*, 5105−5113.
(25) Roiati, V.; Mosconi, E.; Listorti, A.; Colella, S.; Gigli, G.; De Angelis, F. Stark Effect in Perovskite/TiO_2 Solar Cells: Evidence of Local Interfacial Order. *Nano Lett.* **2014**, *14*, 2168−2174.
(26) Tress, W.; Correa Baena, J. P.; Saliba, M.; Abate, A.; Graetzel, M. Inverted Current−Voltage Hysteresis in Mixed Perovskite Solar Cells: Polarization, Energy Barriers, and Defect Recombination. *Adv. Energy Mater.* **2016**, *6*, 1600396.
(27) Domanski, K.; Roose, B.; Matsui, T.; Saliba, M.; Turren-Cruz, S.-H.; Correa-Baena, J.-P.; Roldan Carmona, C.; Richardson, G.; Foster, J.; De Angelis, F.; et al. Hagfeldt, A.; Abate, A., Migration of cations induces reversible performance losses over day/night cycling in perovskite solar cells. *Energy Environ. Sci.* **2017**, *10*, 604.
(28) Bisquert, J. *Nanostructured Energy Devices: Equilibrium Concepts and Kinetics*; CRC Press: Boca Raton, FL, 2014.
(29) Bisquert, J.; Garcia-Belmonte, G.; Mora-Sero, I. Characterization of Capacitance, Transport and Recombination Parameters in Hybrid Perovskite and Organic Solar Cells. In *Unconventional Thin Film Photovoltaics*; Como, E. D., Angelis, F. D., Snaith, H., Walker, A., Eds.; The Royal Society of Chemistry: London, 2016.
(30) Müller, C.; Glaser, T.; Plogmeyer, M.; Sendner, M.; Döring, S.; Bakulin, A. A.; Brzuska, C.; Scheer, R.; Pshenichnikov, M. S.; Kowalsky, W.; et al. Water Infiltration in Methylammonium Lead Iodide Perovskite: Fast and Inconspicuous. *Chem. Mater.* **2015**, *27*, 7835−7841.
(31) Gottesman, R.; Haltzi, E.; Gouda, L.; Tirosh, S.; Bouhadana, Y.; Zaban, A.; Mosconi, E.; De Angelis, F. Extremely Slow Photoconductivity Response of $CH_3NH_3PbI_3$ Perovskites Suggesting Structural Changes under Working Conditions. *J. Phys. Chem. Lett.* **2014**, *5*, 2662−2669.
(32) Gouda, L.; Gottesman, R.; Ginsburg, A.; Keller, D. A.; Haltzi, E.; Hu, J.; Tirosh, S.; Anderson, A. Y.; Zaban, A.; Boix, P. P. Open Circuit Potential Build-Up in Perovskite Solar Cells from Dark Conditions to 1 Sun. *J. Phys. Chem. Lett.* **2015**, *6*, 4640−4645.
(33) Zarazua, I.; Han, G.; Boix, P. P.; Mhaisalkar, S.; Fabregat-Santiago, F.; Mora-Seró, I.; Bisquert, J.; Garcia-Belmonte, G. Surface Recombination and Collection Efficiency in Perovskite Solar Cells from Impedance Analysis. *J. Phys. Chem. Lett.* **2016**, *7*, 5105−5113.
(34) Jeon, N. J.; Noh, J. H.; Kim, Y. C.; Yang, W. S.; Ryu, S.; Seok, S. I. Solvent engineering for high-performance inorganic−organic hybrid perovskite solar cells. *Nat. Mater.* **2014**, *13*, 897−903.
(35) Jeon, N. J.; Noh, J. H.; Yang, W. S.; Kim, Y. C.; Ryu, S.; Seo, J.; Seok, S. I. Compositional engineering of perovskite materials for high-performance solar cells. *Nature* **2015**, *517*, 476−480.
(36) Abate, A.; Leijtens, T.; Pathak, S.; Teuscher, J.; Avolio, R.; Errico, M. E.; Kirkpatrik, J.; Ball, J. M.; Docampo, P.; McPherson, I.; et al. Lithium salts as "redox active" p-type dopants for organic semiconductors and their impact in solid-state dye-sensitized solar cells. *Phys. Chem. Chem. Phys.* **2013**, *15*, 2572−2579.
(37) Abate, A.; Staff, D. R.; Hollman, D. J.; Snaith, H. J.; Walker, A. B. Influence of ionizing dopants on charge transport in organic semiconductors. *Phys. Chem. Chem. Phys.* **2014**, *16*, 1132−1138.

DOI: 10.1021/acsenergylett.7b00059
ACS Energy Lett. 2017, 2, 681−688